ISSN 1062-8738, Bulletin of the Russian Academy of Sciences: Physics, 2021, Vol. 85, No. 6, pp. 632–636. © Allerton Press, Inc., 2021.
Russian Text © The Author(s), 2021, published in Izvestiya Rossiiskoi Akademii Nauk, Seriya Fizicheskaya, 2021, Vol. 85, No. 6, pp. 811–816.

Using Graphics Accelerators in Modeling Nonlinear Ultrasonic Beams on the Basis of the Westervelt Equation

E. O. Konnova[a], *, P. V. Yuldashev[a], and V. A. Khokhlova[a]

[a] *Department of Physics, Moscow State University, Moscow, 119991 Russia*

**e-mail: helen.7aprel@gmail.com*

Received December 9, 2020; revised January 25, 2021; accepted February 26, 2021

Abstract—The problem of accelerating algorithms is considered for calculating the effects of diffraction, nonlinearity, and absorption in modeling high-intensity ultrasonic beams using the nonlinear Westervelt equation. The results from calculations using graphics accelerators (graphical processing units) are compared to ones obtained with a central processing unit. The performance of the algorithm is analyzed as a function of the parameters of the input data.

DOI: 10.3103/S1062873821060125

INTRODUCTION

Noninvasive surgery is a rapidly developing branch of medical acoustics in which powerful focused ultrasonic beams are used to destroy specified structures (e.g., tumors) inside the human body [1]. Nonlinear sound beams must be modeled when designing transducers for generating powerful ultrasound and determining the effectiveness and safety of therapeutic intervention [2]. The emitter in most cases generates a monochromatic wave whose spectrum is enriched with higher harmonics during propagation, due to the effects of acoustic nonlinearity. The nonlinear Westervelt equation is commonly used for modeling ultrasonic beams. A theoretical model based on the Westervelt equation allows us to accurately describe nonlinear shock-wave fields generated by focused high-power ultrasound transducers in homogeneous absorbing media [3, 4]. However, supercomputer power must generally be used to solve this equation when the evolutionary variable is time [5].

Scientists are developing special algorithms for optimizing numerical models of the propagation of nonlinear focused ultrasonic beams. In this work, we consider a directed three-dimensional beam that is of practical importance. We can in this case move to a retarded time coordinate system whose axis is oriented along the preferred direction of wave propagation in the beam (i.e., along the z axis) (Fig. 1). The Westervelt equation therefore takes the form of an evolutionary equation expressing the first derivative of the acoustic pressure along the axial coordinate through a combination of terms that can be considered known for a given z. An equation of this type is normally solved numerically by splitting into physical factors [6], according to which each physical effect is calculated separately at each step along the z coordinate in the preferred direction of wave propagation using a specific procedure. Typical dimensions of the matrices for storing the pressure field can be as high as N_x = 10000 per N_y = 10000 (Fig. 1) for each of the $N_{\max}$ = 1000 harmonics of the nonlinear waveform [7]. Despite these simplifications, the volume of data and the corresponding complexity of the calculations require the use of supercomputers.

The requirements for the amount of RAM can be reduced by optimizing the distribution of higher harmonics in space. This problem can be solved using a

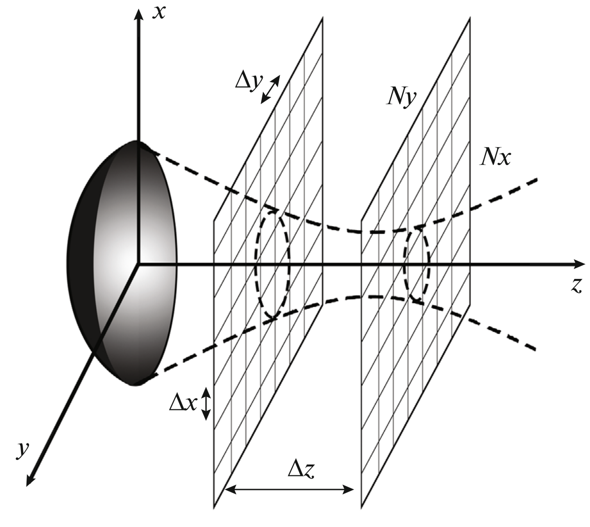

Fig. 1. Scheme of calculations for a nonlinear focused ultrasonic beam.

PC with multicore central processing units (CPU) [7]. However, one calculation can take up to several days, even if the calculations are executed in parallel on several processor cores (usually 2 to 16), which speeds up the calculations by approximately the corresponding number of times. This is because computational operations with large volumes of data must be performed at each step of the algorithm. It is also normally required to make several tens of calculations to characterize the field of one emitter throughout the range of powers [4]. In addition to the speed of calculations, the use of PC calculations is also limited by the processor's RAM. If there is insufficient memory to perform calculations with the available volume of data, there is a hard-disk exchange of data that greatly slows the algorithm and makes calculations impractical. A potential way of solving the problem of computational speed is to use graphical processing units (GPUs) that have as many as several thousand highly specialized cores and allow us to perform a fairly wide range of mathematical operations [8]. However, raising the number of cores does not necessarily speed up computations by the corresponding number of times. This is because GPU cores are less powerful than their CPU counterparts, and their performance and computational speed are correspondingly worse. When each step of the algorithm along the evolutionary coordinate is executed, the data is stored and recorded in the RAM of the CPU. This requires an exchange of data between the CPU and GPU at each step of the algorithm, and this process takes additional time. Due to features of GPU architecture, a major problem is finding a balance between the maximum volumes of data processed at this step of the algorithm (the data are loaded into the GPU RAM in order to avoid their transfer in parts) and minimizing the exchange of data between the CPU RAM and the GPU RAM.

The aim of this work was to develop an algorithm for numerically calculating the effects of acoustic nonlinearity, diffraction, and absorption according to the one-way Westervelt equation, using graphical processing units (GPUs) that help solve the problem of modeling nonlinear ultrasonic beams.

THEORETICAL MODEL

The Westervelt equation in a retarded time coordinate system can be written in evolutionary form as

$$\frac{\partial^2 p}{\partial\tau\partial z} = \frac{c_0}{2}\left(\frac{\partial^2 p}{\partial x^2} + \frac{\partial^2 p}{\partial y^2} + \frac{\partial^2 p}{\partial z^2}\right) + \frac{\beta}{2\rho_0 c_0^3}\frac{\partial^2 p^2}{\partial\tau^2} + \frac{\delta}{2c_0^3}\frac{\partial^3 p}{\partial\tau^3}, \tag{1}$$

where $p(x, y, z, \tau)$ is the acoustic pressure; c_0 is the speed of sound in the medium; $\tau = t - z/c_0$ retarded time; β is a nonlinearity coefficient; and δ is the coefficient of thermoviscous absorption [3, 4]. The differential operators on the right side of the equation, noted from left to right, describe the effects of diffraction, nonlinearity, and thermoviscous absorption.

In the numerical solution to Eq. (1) at each step in the z coordinate, discretized pressure field $p(x, y, z, \tau)$ in the computer's memory takes the form of a three-dimensional matrix that contains a set of complex amplitudes of $N_{\max}$ harmonics of the wave spectrum in the expansion of its waveform into a finite Fourier series at each spatial point of plane xy on a grid with number of points N_x and step Δx along axis x and N_y with step Δy along axis y:

$$p(x, y, z, \tau) = \sum_{n=-N_{\max}}^{N_{\max}} p_n(x, y, z)\, e^{-i\omega_n\tau}, \tag{2}$$

where the angular frequencies of the harmonics are $\omega_n = \omega n$; ω is the angular frequency of the monochromatic source; and p_n are the complex amplitudes of the harmonics. Note that it is sufficient to store only half of the spectrum (at positive frequencies) in the computer memory, since the second half at negative frequencies is complex-conjugate to the first half.

As noted above, this problem takes a long time to solve using CPUs. The use of GPUs is becoming more popular, for which a great number of algorithms have already been adapted. An advantage of GPUs is that they contain up to several thousand small cores that perform many arithmetic operations at the same time, while CPUs contain several powerful cores that execute the widest possible set of operations [8]. Libraries of many standard mathematical operations and procedures such as those related to linear algebra and fast Fourier transform (FFT) have already been introduced for modern GPUs.

Let us consider the physical effects included in Eq. (1) individually. The effect of diffraction is described by the equation [9]

$$\frac{\partial^2 p}{\partial z\partial\tau} = \frac{c_0}{2}\Delta p, \tag{3}$$

where $\Delta = \frac{\partial^2}{\partial x^2} + \frac{\partial^2}{\partial y^2} + \frac{\partial^2}{\partial z^2}$ is the Laplace operator. Diffraction equation (3) for the complex amplitude of one harmonic is written as

$$\frac{\partial p_n}{\partial z} = \frac{i}{2k_n}\Delta p_n, \tag{4}$$

where $k_n = \omega_n/c_0$ is the wave number. When solving Eq. (4) with the angular spectrum approach, the amplitudes of the spatial spectrum are found using a direct FFT from the two-dimensional distribution of harmonic field $p_n(x, y, z)$ at distance z from the source:

$$\widehat{p_n}(k_{x,} k_y, z) = \sum_{m=0}^{N_x-1}\sum_{l=0}^{N_y-1} p_n(x, y, z)\, e^{ik_x x + ik_y y}, \tag{5}$$

where $x = m\Delta x$, $y = l\Delta y$. Multiplying the spectral amplitudes by the propagator corresponding to Eq. (4) yields a solution for the amplitudes on the next plane, which is separated from the previous one by step Δz:

$$\widehat{p_n}(k_x, k_y, z + \Delta z) = \widehat{p_n}(k_x, k_y, z)e^{-i\Delta z k_n + i\Delta z\sqrt{k_n^2 - k_x^2 - k_y^2}}. \quad (6)$$

When performing the inverse FFT, a solution is obtained at the next distance $z + \Delta z$ from the source:

$$p_n(x, y, z + \Delta z) = \frac{1}{N_x N_y}\sum_{0}^{N_x-1}\sum_{0}^{N_y-1}\widehat{p_n}(x, y, z + \Delta z)e^{-ik_x x - ik_y y}. \quad (7)$$

We next consider the effect of thermoviscous absorption, the equation for which is written as

$$\frac{\partial p}{\partial z} = \frac{\delta}{2c_0^3}\frac{\partial^2 p}{\partial \tau^2}. \quad (8)$$

In spectral representation, this equation has an exact analytical solution:

$$p_n(x, y, z + \Delta z) = p_n(x, y, z)\exp\left(-\frac{\Delta z \omega_n{}^2 \delta}{2c_0^3}\right). \quad (9)$$

Nonlinear effects are described by the differential equation

$$\frac{\partial p}{\partial z} = \frac{\beta}{2\rho_0 c_0^3}\frac{\partial p^2}{\partial \tau}. \quad (10)$$

Since the acoustic pressure is presented in the form of a Fourier series in time harmonics (2), Eq. (10) at a given point in space is written in the form of a system of nonlinear coupled equations [10]:

$$\frac{\partial p_n}{\partial z} = \frac{in\omega\beta}{\rho_0 c_0^3}\left(\sum_{k=1}^{N_{\max}-n} p_k p_{n+k}^* + \frac{1}{2}\sum_{k=1}^{n-1} p_k p_{n-k}\right), \quad (11)$$

where p_n^* is the complex-conjugate amplitude of the harmonic. We must therefore solve the system of ordinary differential equations of the first order for the amplitudes of the harmonics in order to calculate the field at next step Δz along axis z. The system can be formulated as the Cauchy problem

$$\frac{d\vec{y}}{dz} = \vec{f}(\vec{y}), \quad \vec{y}(z_0) = \vec{y}_0. \quad (12)$$

The vector of values $\vec{y}$ of size $N_{\max}$ is a set of harmonics at each point in space, and $\vec{f}$ is a function of the harmonic amplitudes on the right-hand side of Eq. (10). An approximate solution to the system at the next $m + 1$ step is constructed using the Runge—Kutta procedure on the fourth order of accuracy [10]:

$$\begin{gathered}\vec{y}_{m+1} = \vec{y}_m + \frac{\Delta z}{6}\left(\vec{k}_1 + 2\vec{k}_2 + 2\vec{k}_3 + \vec{k}_4\right),\\ \vec{k}_1 = \vec{f}(x_m, \vec{y}_m), \quad \vec{k}_2 = \vec{f}\left(x_m + \frac{\Delta z}{2}, \vec{y}_m + \frac{\Delta z}{2}\vec{k}_1\right),\\ \vec{k}_3 = \vec{f}\left(x_m + \frac{\Delta z}{2}, \vec{y}_m + \frac{\Delta z}{2}\vec{k}_2\right),\\ \vec{k}_4 = \vec{f}\left(x_m + \Delta z, \vec{y}_m + \Delta z\vec{k}_3\right).\end{gathered} \quad (13)$$

The calculations are repeated in a computational cycle until the required interval along the z axis is passed. Splitting according to physical factors of the second order of accuracy is in this case used [13]. This means the diffraction and absorption operators at step $\Delta z/2$ are first calculated at each step of the cycle. The nonlinearity operator at full step Δz is then calculated, and the calculations for the first two operators at the half step are repeated again.

Our calculations were made using an Intel Core i7 4790 CPU (four physical cores and eight virtual cores) and the GPU of an Nvidia GTX1070 video card, for which a program was written in C that included the functions of the CUDA kernel, which implemented algorithms (6), (9), and (13), respectively. Two-dimensional Fourier transforms required when using an angular spectrum were performed using the built-in cuFFT library from the Cuda Development Toolkit package. Parallel execution was achieved due to both the internal parallelism of the fast Fourier transform algorithm implemented for the GPU and to the execution of the CUDA kernel function when multiplying the spatial spectrum by propagator (6). The absorption and nonlinearity algorithms were parallelized along the spatial coordinates of plane *xy*. The cores of the multicore processor calculated in parallel the absorption and nonlinearity operators for different points in the space of plane *xy*. In the CPU algorithm, parallel calculations of diffraction were achieved via the simultaneous processing of the fields of several harmonics by the CPU cores according to algorithm (5)—(7).

RESULTS AND DISCUSSION

The initial distribution of the complex amplitude of the first harmonic in plane $z = 0$ was obtained using the Rayleigh integral in [14], calculated for a focused transducer with a frequency of 1 MHz, a diameter of 10 cm, and a focal length of 9 cm [12]. The distribution was specified on a square grid with total number of cells N_xN_y, where $N_x = N_y = 2560$. The spatial step was $\Delta x = \Delta y = 0.4$ mm, and the number of harmonics used in the calculations was $N_{\max} = 50$. The algorithm's operation provided the distributions of the first three field harmonics on the emitter's axis (Fig. 2), and in the focal (Figs. 3a—3c) and axial (Figs. 3d—3f) planes. The calculated spatial distributions of the harmonic

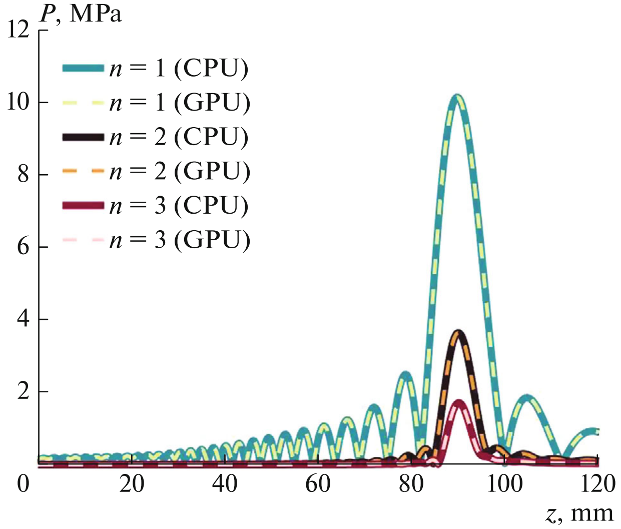

Fig. 2. Amplitudes of the first three harmonics on the axis of the emitter.

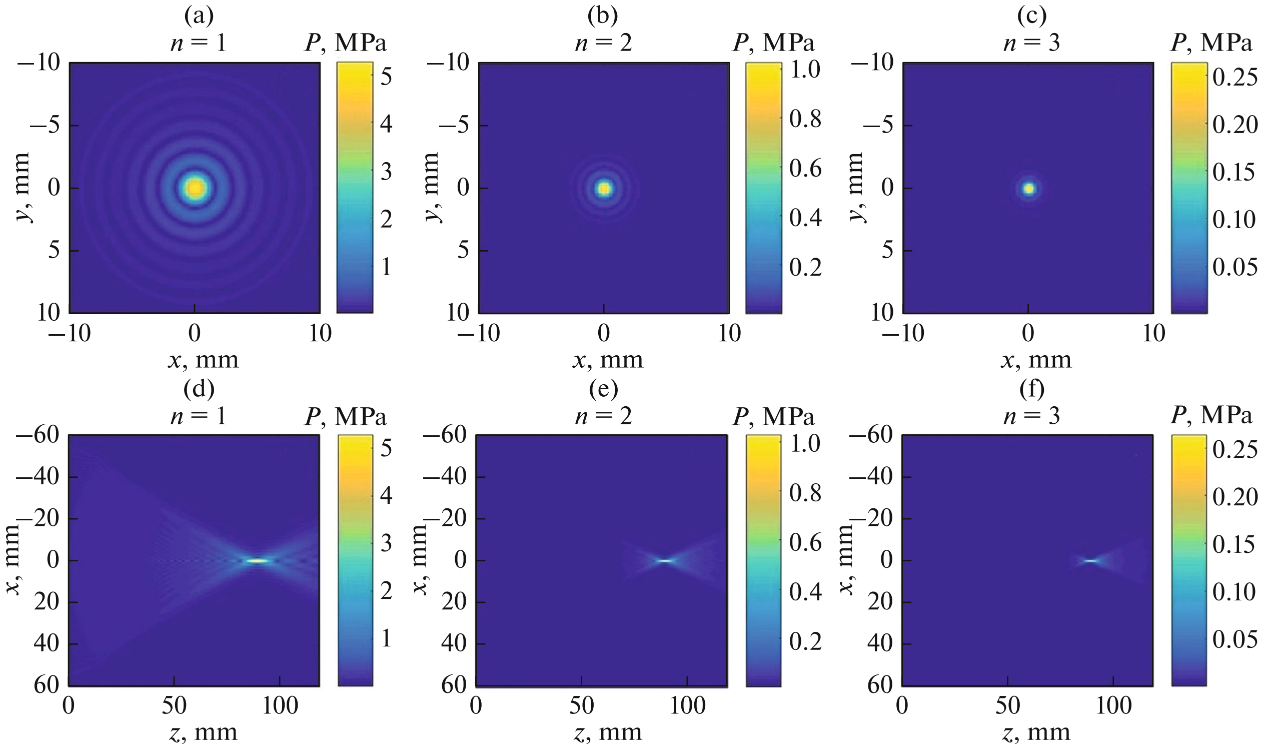

Fig. 3. Amplitude distribution of the (a) first, (b) second, and (c) third harmonics in the focal plane. The amplitude distribution of the (d) first, (e) second, and (f) third harmonics in the plane of the beam's axis.

amplitudes were compared to ones obtained in the program executed using the CPU. Both calculations gave indistinguishable results, confirming the correctness of the algorithm implemented for the GPU.

Table 1 compares the running time of a single-threaded algorithm executed using the CPU with multi-threaded algorithms and an algorithm using the GPU with a beam propagation of 1200 steps (or 120 mm). Calculations can be sped up by around an order of magnitude using the GPU, compared to the eight-thread algorithm using the CPU (even though the GPU has hundreds of times more cores). This is because the difference between the power of the pro-

Table 1. Comparison of the speeds of execution for all types of algorithms

Matrix dimension N_x, N_y	Number of harmonics $N_{\max}$	T, min			
		One CPU thread	Four CPU threads	Eight CPU threads	GPU (1920 threads)
2560	10	1900	470	300	23
	50	43200	11520	7800	252

Table 2. Comparison of the speed of execution for algorithms with eight CPU threads and GPU threads for different numbers of harmonics

Number of harmonics $N_{\max}$		10	30	50	80	100
T, s	Eight CPU threads	137	1100	3350	9850	16300
	GPU (1920 threads)	12.2	56	128	285	423
T_8/T_{GPU}		12	20	26	35	39

cessor cores and the time spent on the exchange of data between the CPU and GPU. Note the speed of calculations using the GPU, compared to that of calculations using eight CPU threads for a different number of harmonics (Table 2). We can see that acceleration grows in proportion to the increase in the number of harmonics. Since that the calculations in both algorithms are based on a set of the simplest arithmetic operations for a large volume of data, the algorithm for the GPU runs faster because there are more parallel threads, despite the lower power of the cores of the processor. Acceleration therefore grows along with the volume of data by, e.g., increasing the number of harmonics.

CONCLUSIONS

The example of calculating the field generated by a focusing ultrasonic emitter was employed to demonstrate the use of computations using GPUs to parallelize the algorithm for solving the Westervelt equation. This version of the algorithm using the GPU sped up calculations by an order of magnitude, compared to the one using the CPU. We plan to optimize the algorithm for the GPU in order to accelerate computations even more.

FUNDING

This work was supported by the Russian Foundation for Basic Research, project no. 20-32-70142.

REFERENCES

1. Beili, M.R., Khokhlova, V.A., Sapozhnikov, O.A., et al., *Acoust. Phys.*, 2003, vol. 49, no. 4, p. 369.
2. Rosnitskiy, P.B., Yuldashev, P.V., Sapozhnikov, O.A., et al., *IEEE Trans. Ultrason., Ferroelectr., Freq. Control*, 2017, vol. 64, no. 2, p. 374.
3. Westervelt, P.J., *J. Acoust. Soc. Am.*, 1963, vol. 35, no. 4, p. 535.
4. Kreider, W., Yuldashev, P.V., Sapozhnikov, O.A., et al., *IEEE Trans. Ultrason., Ferroelectr., Freq. Control*, 2013, vol. 60, no. 8, p. 1683.
5. Okita, K., Ono, K., Takagi, S., and Matsumoto, Y., *Int. J. Numer. Methods Fluids*, 2010, vol. 65, nos. 1–3, p. 43.
6. Ames, W.F., *Numerical Methods for Partial Differential Equations*, San Diego: Academic, 1992.
7. Yuldashev, P.V. and Khokhlova, V.A., *Acoust. Phys.*, 2011, vol. 57, no. 3, p. 334.
8. Perepelkin, E.E., Sadovnikov, B.I., and Inozemtseva, N.G., *Vychisleniya na graficheskikh protsessorakh (GPU) v zadachakh matematicheskoi i teoreticheskoi fiziki* (Computing Using Graphic Processors (GPU) in Problems of Mathematical and Theoretical Physics), Moscow: Lenand, 2014.
9. Konnova, E.O., Yuldashev, P.V., and Khokhlova, V.A., in *Sb. tr. XVII Vseross. shkoly-seminara "Volny-2019"* (Proc. XVII All-Russian School-Seminar "Waves-2019"), Moscow, 2019, p. 10.
10. Kashcheeva, S.S., Sapozhnikov, O.A., Khokhlova, V.A., et al., *Acoust. Phys.*, 2000, vol. 46, no. 2, p. 170.
11. Kalitkin, N.N., *Chislennye metody* (Numerical Methods), Moscow: Nauka, 1978.
12. Mezdrokhin, I.S., Yuldashev, P.V., and Khokhlova, V.A., *Acoust. Phys.*, 2018, vol. 64, no. 3, p. 309.
13. Zemp, R.J., Tavakkoli, J., and Cobbold, R.S.C., *J. Acoust. Soc. Am.*, 2003, vol. 113, no. 1, p. 139.
14. Neil, H.T., *J. Acoust. Soc. Am.*, 1949, vol. 21, no. 5, p. 516.

Translated by I. Obrezanova